Impact of the Buffer Layers and Anodization on Properties of NbTiN Films for THz Receivers

Elena S. Zhukova, Boris P. Gorshunov, Lenar S. Kadyrov, Kirill V. Zhivetev, Andrii V. Terentiev, Artem M. Chekushkin, Fedor V. Khan, Andrey V. Khudchenko, Nickolay V. Kinev, and Valery P. Koshelets

***Abstract*—In this article, we present the results of the research aimed at improving the fabrication process of a SIS-mixer for operation at frequencies close to 1 THz. We study the impact of buffer aluminum oxide layer and anodization effects on the properties of superconducting NbTiN films which form the electrodes of the transmission lines in THz-range devices. These layers are traditionally used in technological processes. The measurements of THz response are performed using terahertz time-domain spectrometer at frequencies from 0.3 to 2.0 THz. It was found that the critical temperature, normal-state conductivity just above the transition temperature, superconducting gap value and London penetration depth of the NbTiN film sputtered on aluminum oxide buffer layer are almost the same as of the film sputtered directly onto the substrate. The difference between the parameters is comparable to the measurement uncertainty for NbTiN films with and without additional surface layers of aluminum and anodization.**

***Index Terms*—Superconducting device fabrication, terahertz radiation, materials testing, niobium compounds, Josephson mixers.**

I. Introduction

MIXERS based on superconductor-insulator-superconductor (SIS) tunnel junctions are widely used in various applications and fundamental research. The area of application includes ground-based [1], [2] and space-based [3], [4] radio astronomy, the monitoring of the atmosphere [5], gas mixture composition study [6], investigation of human body in THz range [7] and others. State-of-the-art mixers have a noise temperature approaching quantum limit value ($T_n = hf/2k_B$) which makes them invaluable for low-power signal detection in terahertz (THz) frequency range; here h is Plank constant, f is the operating frequency and k_B is Boltzmann constant.

Most of the SIS-mixers are fabricated using Nb technology [8], [9], [10] which allows to cover an entire frequency range up to 700 GHz. At higher frequencies the photon energy hf exceeds the twice gap energy 2Δ of Nb and losses in the electrodes of the transmission lines cause a deterioration of the receiver performance [11]. Nb compounds with higher energy gap (e.g., NbN and NbTiN) are used in order to overcome this frequency limitation.

Research on properties of superconducting NbTiN films was performed by a number of scientific groups [12], [13], [14], [15], [16]. The optimal manufacturing conditions and recommendations on how to improve the quality of the films were suggested by the authors, as well as the measurement techniques used to characterize the films [12], [17], [18], [19].

In our previous papers we began to study the properties of superconducting NbTiN films aiming to take into account as much technological factors as possible. We have already tested the properties of the films produced at different pressure of nitrogen while sputtering [20] and studied the effect of the substrate [21]. Also we have compared both TDS and FTS results and found that TDS is more suitable for studying NbTiN films due to better signal-to-noise ratio [22].

In this work we make the next step towards the fabrication of near 1 THz SIS-mixer and study the effect of buffer layer and anodization on the properties of the NbTiN films. In Section II the fabrication process of the superconducting devices based on SIS tunnel junctions is described. The information on the samples studied in this work can be found here as well. Section III presents the TDS measurement results and the discussion.

II. Fabrication Technology

Fabrication process of the superconducting devices involves several stages of sputtering and etching [23]. The schematic representation of the layer structure near SIS junction embedded into transmission line is shown in Fig. 1. Etching of Nb and NbN layers in CF_4 plasma is used in order to form SIS tunnel junctions. The layer of aluminum nitride which forms the barrier is removed using rf-ion or ICP etching. Additional layer of Al on the surface of NbTiN bottom electrode serves as a stop-layer

Manuscript received 26 September 2023; revised 14 December 2023 and 31 December 2023; accepted 31 December 2023. Date of publication 16 January 2024; date of current version 26 January 2024. This work was supported in part by Russian Science Foundation under Grant 23-79-00019. TDS measurements were performed within State Task of Ministry of Science and Higher Education of the Russian Federation under Grant FSMG-2021-0005 (https://rscf.ru/project/23-79-00019/). *(Corresponding author: Fedor V. Khan.)*

Elena S. Zhukova, Boris P. Gorshunov, Lenar S. Kadyrov, Kirill V. Zhivetev, and Andrii V. Terentiev are with the Moscow Institute of Physics and Technology, National Research University, 141701 Dolgoprudny, Russia (e-mail: zhukova.es@mipt.ru; bpgorshunov@gmail.com; kadyrov.ls@mipt.ru; zhivetev.kv@phystech.edu; terentev.a@phystech.edu).

Artem M. Chekushkin, Fedor V. Khan, Nickolay V. Kinev, and Valery P. Koshelets are with the Kotelnikov Institute of Radio Engineering and Electronics, Russian Academy of Sciences, 125009 Moscow, Russia (e-mail: chekushkin@hitech.cplire.ru; khanfv@hitech.cplire.ru; nickolay@hitech.cplire.ru; valery@hitech.cplire.ru).

Andrey V. Khudchenko is with the Astro Space Center of Lebedev Physical Institute, Russian Academy of Sciences, 119991 Moscow, Russia (e-mail: khudchenko@asc.rssi.ru).

Color versions of one or more figures in this article are available at https://doi.org/10.1109/TASC.2024.3353139.

Digital Object Identifier 10.1109/TASC.2024.3353139

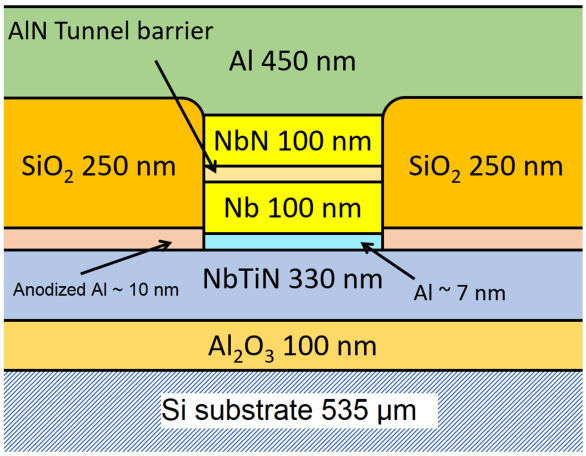

Fig. 1. Schematic representation of the layer structure near the SIS-junction in NbTiN-Al embedding circuit.

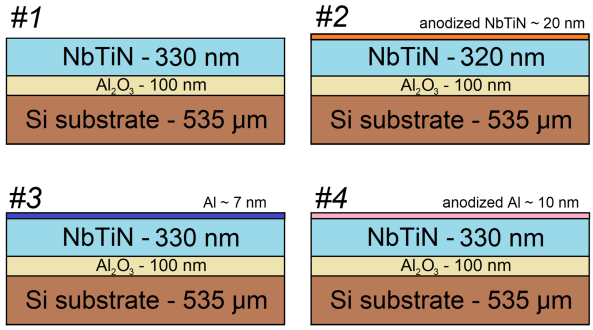

Fig. 2. Illustration of the samples under study. All the films are sputtered on Al_2O_3 buffer layer. #1 is NbTiN film; #2 is NbTiN film with anodized surface; #3 is NbTiN film with Al layer on the top; #4 is the film covered with Al layer and anodized.

TABLE I
PARAMETERS OF SUPERCONDUCTING NBTIN FILMS

	d, nm	$\sigma_{0,\,DC}$, 10^4 $(\Omega\cdot cm)^{-1}$	$T_{c,\,DC}$, K	$\sigma_{0,\,TDS}$, 10^4 $(\Omega\cdot cm)^{-1}$	$T_{c,TDS}$, K	$2\Delta_0$, *meV*	λ_0, *nm*
#1	330	1.03	15.1	1.09	13.9	5.0	283
#2	340	n.a.	n.a.	1.00	13.7	4.7	310
#3	340	n.a.	n.a.	1.07	13.8	4.8	295
#4	340	n.a.	n.a.	1.01	13.7	4.8	300
[20] #5	338	1.07	15.2	1.12	13.8	5.2	282

for etching in CF_4 and for the flattening of the film surface [24], [25], [26]. During the etching processes the surface of the substrate also deteriorates unless the Al_2O_3 layer between silicon and NbTiN is used. Moreover, NbTiN film sputtered on the amorphous Al_2O_3 layer can potentially have better properties compared to the film on bare silicon as NbTiN and silicon have different lattice parameters [15].

In our quasioptical SIS-mixers, slot lines and slot antennas are commonly used [27], [28]. The thickness of the insulator in microstrip lines may also vary to provide better impedance matching between the circuit components. The thickness of the insulator is comparable to the thickness of the electrodes. In this geometry, top and bottom electrodes can overlap and short-circuit the line near the slot.

In order to prevent the shorts anodization process is used. It is performed by putting the films into electrolyte and applying positive voltage. The thickness of the anodization layer depends on the applied voltage and the type of material. When a voltage of 10 V is applied to the film, 9 nm of aluminum on the surface turn into 13-nm-thick aluminum oxide layer. At the same conditions, 9 nm of Nb turn into anodization layer with thickness of about 23 nm [29], [30].

In order to study the effects of the additional layers and anodization both independently and mutually, we produced a series of samples shown in Fig. 2. All the samples were fabricated on high-resistivity silicon substrate using cluster magnetron system Kurt J. Lesker. Al_2O_3 buffer layer was obtained by rf-magnetron sputtering from Al_2O_3 target with 99.95% purity. NbTiN film was sputtered on the top of buffer layer under the same conditions as the sample #5 described in [19]. In order to exclude the discrepancies which may arise due to sputtering processes being performed separately, Al_2O_3 and NbTiN layers were sputtered on a single substrate which was then cut into pieces with in-plane dimensions of 7×7 mm^2.

Sample #1 is NbTiN film sputtered on Al_2O_3 buffer layer. Sample #2 is the same NbTiN film with anodized surface. Top surface of the sample #3 is covered with 7 nm-thick aluminum layer. Sample #4 is the same as sample #3, but with anodized surface. It should also be noted, that samples #1 and #3 also have thin (1–2 nm) oxide film on the surface due to atmospheric oxygen.

Values of the critical temperature T_c and normal-state conductivity σ_0 near T_c obtained from the DC-measurements using 4-probe technique are $T_c = 15.1$ K and $\sigma_0 = 1.0{\cdot}10^4\ \Omega^{-1}\text{cm}^{-1}$ for the sample #1. The geometry of the test sample for DC-measurements is a 20 μm-wide and 1 mm-long strip (50 squares). Test sample was fabricated on the separate chip, but in one technological cycle with the samples prepared for study using TDS

III. TDS MEASUREMENTS

A. *Measurements and Models*

The fabricated samples were studied using THz time-domain spectrometer TeraView TPS Spectra 3000. First, bare silicon substrate was examined in order to obtain its permittivity and exact thickness values. Second, transmission coefficient spectra of the samples #1 and #2 were measured in frequency range 0.3–2.0 THz and at temperatures from 5 K up to 16 K.

We used the expressions by Zimmermann et al. [31] to calculate complex conductivity of the superconducting films. The presence of the 100 nm-thick Al_2O_3 buffer layer causes a significant phase shift of a signal. Therefore, we had to model three-layer system rather than two-layer, as it was in our previous studies [20], [21], [22]. The expression for transmission coefficient of a three-layer system in general case is given in Appendix.

The measurement results for the sample #2 are shown in Fig. 3. The spectra for the samples #1, #3, #4 are similar to those of #2 and are not shown (see Table I for the parameters). Spectra of the real part of conductivity and permittivity (Fig. 3(b) and (c), respectively) were obtained from the spectra of complex

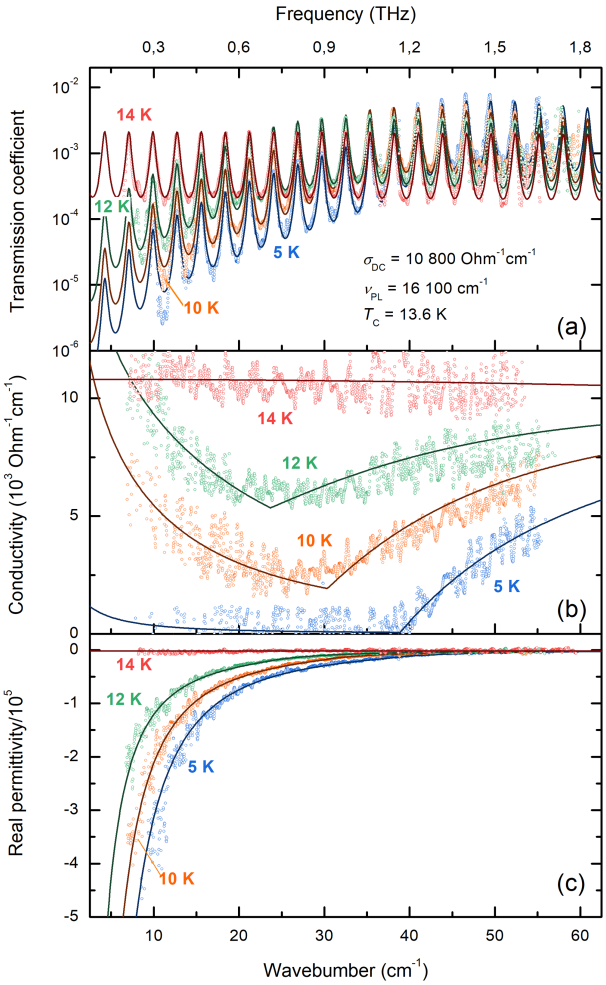

Fig. 3. Typical spectra of (a) transmission coefficient; (b) real part of conductivity; (c) real part of permittivity of the superconducting films on insulator substrate. Experimentally measured data points are marked with dots. Solid lines represent the model curves as described in the text. Parameters indicated in panel (a) are: σ_{DC}, $\nu_{\rm PL}$ – conductivity and plasma frequency of charge carriers in normal state at temperature just above critical temperature T_c, respectively.

transmission coefficient (Fig. 3(a)) using TeraCalc software [32].

The following parameters of the films were obtained for each fixed temperature by fitting the experimental curves shown in Fig. 3: Δ and λ_L which denote the superconducting gap energy, and London penetration depth, respectively; σ_0 is determined here as well. Temperature dependences of Δ and λ_L are shown in Fig. 4. Data points are marked with dots. Solid lines represent model fitting to the data.

We used an empirical expression for fitting $\Delta(T)$ and two-fluid model formula for $\lambda_L(T)$:

$$\Delta = \Delta_0 \tanh\left(1.74\sqrt{\frac{T_c}{T}-1}\right) \quad (1)$$

$$\lambda_L = \lambda_0 \sqrt{1-\left(\frac{T}{T_c}\right)^4}, \quad (2)$$

where Δ_0 and λ_0 are the zero-temperature values of the superconducting gap and the London penetration depth, respectively. The models show good agreement with the experimental data.

B. Discussion

Data in Fig. 4 display the impact of the anodization and of aluminum surface layers on Δ and λ_L. Both Δ and λ_L values of all 4 samples are comparable within the experimental uncertainty. However, in Fig. 4(a) and (d), small systematic shift between the data points corresponding to samples #1 and #2 can be observed. This shift may be caused either by proximity effect or by deterioration of the quality of the film surface after anodization of NbTiN. Direct study of the surface is currently being carried out and will be published elsewhere.

Additional aluminum layer (#3) leads to slightly smaller Δ and larger λ_L compared to those values of bare NbTiN film (#1), most likely due to proximity effect (see Fig. 4(b) and (e)). NbTiN film with anodized aluminum on the top has almost the same parameters as the one with aluminum without anodization (Fig. 4(c) and (f)). The observed minor impact of the layer can be explained by small relative variation of the films thickness.

The values of the parameters of the samples obtained from fitting the data shown in Figs. 3 and 4 are listed in Table I. We compare them with the results of the previous paper where NbTiN films on bare silicon substrates were studied (see film #5 in [20]). DC-results are also presented here.

We found that T_c, λ_0 and σ_0 values obtained for NbTiN films with and without Al_2O_3 layer are equal within the experimental uncertainty, and Δ is smaller for the film on Al_2O_3. That is different from what we expected and what was observed in [15]. The films in our study have a large thickness about 340 nm, and impact of the buffer layer is negligible except for the layers closest to film–buffer layer interface.

T_c value measured by DC-probe is different from that obtained using TDS, probably due to strong inhomogeneity of the film parameters at temperatures close to T_c [20]. There are superconducting 'grains' partly separated by the areas that are in normal state. DC-current can flow along the pattern formed by the superconducting regions, which is not the case for the alternating current at terahertz frequencies. Therefore, effective critical temperature at which the entire film is in a superconducting state will be lower compared to the value measured by DC-probe.

IV. Conclusion

To sum up, we found out that the properties of the films are not affected by the Al_2O_3 buffer layer which is needed for technological process. The anodized aluminum layer on the top surface of the NbTiN film which is used as a stop-layer for etching process has only minor impact on T_c, σ_0, λ_0 and Δ_0 values. It is important, that all these parameters were obtained by TDS spectroscopic measurements and are much more relevant for high-frequency applications than regular DC data.

In a recent work [33], the described technological process was successfully used for fabrication of the superconducting on-chip

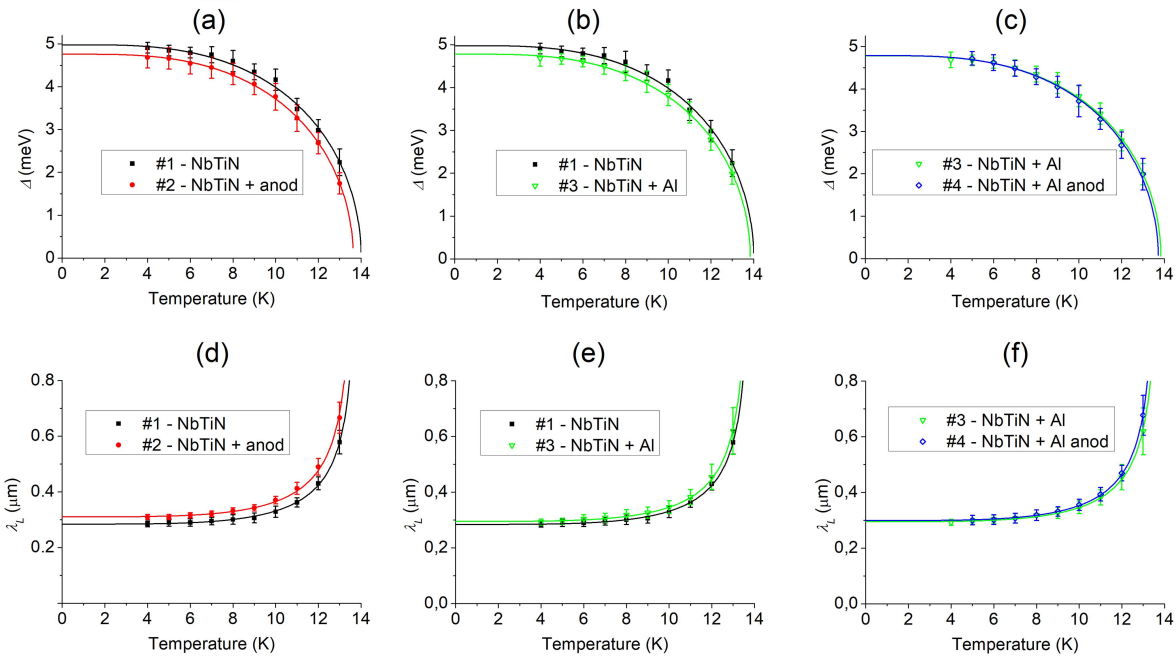

Fig. 4. Temperature dependences of the superconducting gap parameter Δ (a), (b), (c); and London penetration depth λ_L (d), (e), (f) of the samples. Panels (a), (d) represent the impact of the anodization layer on the top of NbTiN film; panels (b), (e) depict the influence of Al; panels (c), (f) show the data for NbTiN film with anodized and pure Al covers.

mixers with NbTiN-Al transmission line and Nb/Al-AlN/NbN tunnel junctions embedded into the line. The measurements of the manufactured samples demonstrated their applicability as mixers at 1.0–1.1 THz frequency range.

APPENDIX

The complex transmission coefficient of a three-layer system is given by the following expression [34], [35]:

$$T^*_{12345} = T_{12}T_{23}T_{34}T_{45}\exp\left(i\left(\delta_2+\delta_3+\delta_4\right)\right)/W, \qquad (3)$$

where

$$\begin{aligned} W &= 1 + W_1 + W_2 + W_3 \\ W_1 &= R_{12}\,R_{23}\exp\left(2i\delta_2\right) + R_{23}R_{34}\exp\left(2i\delta_3\right) \\ &\quad + R_{34}R_{45}\exp\left(2i\delta_4\right) \\ W_2 &= R_{12}\,R_{34}\exp\left(2i\left(\delta_2+\delta_3\right)\right) \\ &\quad + R_{23}R_{45}\exp\left(2i\left(\delta_3+\delta_4\right)\right) \\ W_3 &= R_{12}\,R_{45}\exp\left(2i\left(\delta_2+\delta_3+\delta_4\right)\right) \\ &\quad + R_{12}R_{23}R_{34}R_{45}\exp\left(2i\left(\delta_2+\delta_4\right)\right) \end{aligned}$$

Here the indices '1' and '5' refer to the media on both sides of the system composed by three layers with indices $2,3,4$ in direction of the wave propagation. The remaining notations in the expression are as follows. A medium with index p is characterized [33] by a complex refractive index ${n_p}^* = n_p + ik_p$; and optical thickness δ_p is given by the expression:

$$\delta_p = 2\pi d_p\left(n_p + ik_p\right)/\lambda$$

Here d_p $(p = 2,3,4)$ are the thicknesses of layers $2,3,4$, and λ is radiation wavelength in vacuum. In our case, layer 2 is silicon substrate ($d_2 = 530$ μm), layer 3 is amorphous Al_2O_3 ($d_3 = 100$ nm), and layer 4 is the superconducting NbTiN film ($d_4 = 330$ nm).

$T_{p,q}$ and $R_{p,q}$ (p, $q = 1,2,3,4,5$) are complex Fresnel reflection and transmission coefficients of an electromagnetic wave at the interface between media with indices p and q:

$$T_{pq} = t_{pq}\,\exp\left(i\varphi^T_{pq}\right), \quad R_{pq} = r_{pq}\,\exp\left(i\varphi^R_{pq}\right)$$

with $t_{p,q}$, $r_{p,q}$ and ${\varphi^T}_{p,q}$, ${\varphi^R}_{p,q}$ defined by formulae:

$$\begin{aligned} t^2_{pq} &= \frac{4\left(n_p^2+n_q^2\right)}{\left(n_p+n_q\right)^2+\left(k_p+k_q\right)^2} \\ r^2_{pq} &= \frac{\left(n_p-n_q\right)^2+\left(k_p-k_q\right)^2}{\left(n_p+n_q\right)^2+\left(k_p+k_q\right)^2} \\ \varphi^T_{pq} &= \arctan\left(\frac{k_pn_q-k_qn_p}{n_p^2+k_p^2+n_pn_q+k_pk_q}\right) \\ \varphi^R_{pq} &= \arctan\left(\frac{2\left(k_pn_q-k_qn_p\right)}{n_p^2+k_p^2-n_q^2-k_q^2}\right) \end{aligned}$$

By analyzing with expression (3) the experimental spectra with the dielectric parameters of silicon substrate and of Al_2O_3 layer measured separately, we found that the thin Al_2O_3 layer practically did not influence the magnitude of the transmission coefficient of the samples. This allowed us to use the TeraCalc software [31] to determine the THz spectra of permittivity and conductivity of the SC film. The software allows determination of real n and imaginary k parts of complex refraction index of the film by solving a system of two nonlinear equations for the amplitude $T(n, k)$ and phase $\varphi^{\mathrm{T}}(n, k)$ of the complex transmission coefficient $T(n, k)\exp[i\varphi^{\mathrm{T}}(n, k)]$ of a two-layered system (film on a substrate). Note that TDS technique allows

for determination of both, the value of transmission coefficient amplitude T and the phase shift φ^{T} of the radiation passed through the sample. Having determined n and k of the film, all other optical parameters can be calculated.

REFERENCES

[1] ALMA Observatory, 1999. Accessed: Sep. 25, 2023. [Online]. Available: https://almaobservatory.org/

[2] APEX Telescope, 2003. Accessed: Sep. 25, 2023. [Online]. Available: https://apex-telescope.org

[3] Hershel Space Observatory, 2009. Accessed: Sep. 25, 2023. [Online]. Available: https://www.herschel.caltech.edu

[4] Millimetron Space Observatory, 2020. Accessed: Sep. 25, 2023. [Online]. Available: https://millimetron.ru

[5] G. De Lange et al., "Development and characterization of the superconducting integrated receiver channel of the TELIS atmospheric sounder," *Supercond. Sci. Technol.*, vol. 23, no. 4, Mar. 2010, Art. no. 045016, doi: 10.1088/0953-2048/23/4/045016.

[6] N. V. Kinev et al., "Terahertz spectroscopy of gas absorption using the superconducting flux-flow oscillator as an active source and the superconducting integrated receiver," *Sensors*, vol. 20, no. 24, Dec. 2020, Art. no. 7267, doi: 10.3390/s20247267.

[7] K. A. Baksheeva et al., "The sub-THz emission of the human body under physiological stress," *IEEE Trans. Terahertz Sci. Technol.*, vol. 11, no. 4, pp. 381–388, Jul. 2021, doi: 10.1109/TTHZ.2021.3066099.

[8] J. D. Garrett, B.-K. Tan, C. Chaumont, F. Boussaha, and G. Yassin, "A 230-GHz endfire SIS mixer with near quantum-limited performance," *IEEE Microw. Wireless Compon. Lett.*, vol. 32, no. 12, pp. 1435–1438, Dec. 2022, doi: 10.1109/LMWC.2022.3190701.

[9] T. Kojima et al., "Three quanta sensitivity superconductor–insulator–superconductor mixer for the 0.78–0.95 THz band," *Appl. Phys. Exp.*, vol. 2, no. 10, Oct. 2009, Art. no. 102201, doi: 10.1143/APEX.2.102201.

[10] K. I. Rudakov et al., "Low-noise sis receivers for new radio-astronomy projects," *Radiophys Quantum El*, vol. 62, pp. 547–555, Mar. 2020, doi: 10.1007/s11141-020-10001-7.

[11] D. C. Mattis and J. Bardeen, "Theory of the anomalous skin effect in normal and superconducting metals," *Phys. Rev.*, vol. 111, no. 2, pp. 412–417, Feb. 1958, doi: 10.1103/PhysRev.111.412.

[12] Y. Uzawa et al., "Tuning circuit material for mass-produced terahertz SIS receivers," *IEEE Trans. Appl. Supercond.*, vol. 25, no. 3, Jun. 2015, Art. no. 2401005, doi: 10.1109/TASC.2014.2386211.

[13] L. Yu et al., "Fabrication of niobium titanium nitride thin films with high superconducting transition temperatures and short penetration lengths," *IEEE Trans. Appl. Supercond.*, vol. 15, no. 1, pp. 44–48, Mar. 2005, doi: 10.1109/TASC.2005.844126.

[14] B. G. C. Bos et al., "Reactive magnetron sputter deposition of superconducting niobium titanium nitride thin films with different target sizes," *IEEE Trans. Appl. Supercond.*, vol. 27, no. 4, Jun. 2017, Art. no. 1500405, doi: 10.1109/TASC.2016.2631939.

[15] T. Shiino et al., "Improvement of the critical temperature of superconducting NbTiN and NbN thin films using the AlN buffer layer," *Supercond. Sci. Technol.*, vol. 23, no. 4, Mar. 2010, Art. no. 045004, doi: 10.1088/0953-2048/23/4/045004.

[16] J. Zichi et al., "Optimizing the stoichiometry of ultrathin NbTiN films for high-performance superconducting nanowire single-photon detectors," *Opt. Exp.*, vol. 27, no. 19, pp. 26579–26587, Sep. 2019, doi: 10.1364/OE.27.026579.

[17] M. Dressel, N. Drichko, B. Gorshunov, and A. Pimenov, "THz spectroscopy of superconductors," *IEEE J. Sel. Topics Quantum Electron.*, vol. 14, no. 2, pp. 399–406, Mar./Apr. 2008, doi: 10.1109/JSTQE.2007.910764.

[18] R. C. Taber, "A parallel plate resonator technique for microwave loss measurements on superconductors," *Rev. Sci. Instrum.*, vol. 61, no. 8, pp. 2200–2206, Aug. 1990, doi: 10.1063/1.1141389.

[19] J. Verjauw et al., "Investigation of microwave loss induced by oxide regrowth in high-Q niobium resonators," *Phys. Rev. Appl.*, vol. 16, no. 1, Jul. 2021, Art. no. 014018, doi: 10.1103/PhysRevApplied.16.014018.

[20] F. V. Khan et al., "Characterization of microwave properties of superconducting NbTiN films using TDS," *IEEE Trans. Terahertz Sci. Technol.*, vol. 13, no. 6, pp. 627–632, Nov. 2023, doi: 10.1109/TTHZ.2023.3321252.

[21] B. N. R. Lap et al., "Characterization of superconducting NbTiN films using a dispersive Fourier transform spectrometer," *Appl. Phys. Lett.*, vol. 119, no. 15, Sep. 2021, Art. no. 152601, doi: 10.1063/5.0066371.

[22] A. Khudchenko et al., "Dispersive spectrometry at terahertz frequencies for probing the quality of NbTiN superconducting films," *IEEE Trans. Appl. Supercond.*, vol. 32, no. 4, Jun. 2022, Art. no. 1500506, doi: 10.1109/TASC.2022.3147736.

[23] A. M. Chekushkin et al., "Optimization of fabrication processes for Nb, NbN, NbTiN films and high-quality tunnel junctions for terahertz receiving circuits," *Tech. Phys.*, vol. 92, no. 13, pp. 2136–2140, Jul. 2022, doi: 10.21883/TP.2022.13.52234.135-21.

[24] T. Imamura and S. Hasuo, "Cross-sectional transmission electron microscopy observation of Nb/AlO_x-Al/Nb Josephson junctions," *Appl. Phys. Lett.*, vol. 58, no. 6, pp. 645–647, Nov. 1991, doi: 10.1063/1.104556.

[25] T. Imamura and S. Hasuo, "Fabrication of high quality Nb/AlO/sub x/-Al/Nb Josephson junctions. II. Deposition of thin Al layers on Nb films," *IEEE Trans. Appl. Supercond.*, vol. 2, no. 2, pp. 84–94, Jun. 1992, doi: 10.1109/77.139224.

[26] N. Rando et al., "Transmission electron microscopy and atomic force microscopy analysis of Nb-Al-AlOx-Nb superconducting tunnel junction detectors," *J. Appl. Phys.*, vol. 77, no. 8, pp. 4099–4106, Apr. 1995, doi: 10.1063/1.359492.

[27] N. V. Kinev, K. I. Rudakov, L. V. Filippenko, A. M. Baryshev, and V. P. Koshelets, "Terahertz source radiating to open space based on the superconducting flux-flow oscillator: Development and characterization," *IEEE Trans. Terahertz Sci. Technol.*, vol. 9, no. 6, pp. 557–564, Nov. 2019, doi: 10.1109/TTHZ.2019.2941401.

[28] V. P. Koshelets and S. V. Shitov, "Integrated superconducting receivers," *Supercond. Sci. Technol.*, vol. 13, no. 5, pp. R53–R69, Jan. 2000, doi: 10.1088/0953-2048/13/5/201.

[29] X. Meng and T. Van Duzer, "Light-anodization process for high-J/sub c/micron and submicron superconducting junction and integrated circuit fabrication," *IEEE Trans. Appl. Supercond.*, vol. 13, no. 2, pp. 91–94, Jun. 2003, doi: 10.1109/TASC.2003.813652.

[30] A. Mozalev et al., "Formation–structure–properties of niobium-oxide nanocolumn arrays via self-organized anodization of sputter-deposited aluminum-on-niobium layers," *J. Mater. Chem. C*, vol. 2, no. 24, pp. 4847–4860, Apr. 2014, doi: 10.1039/C4TC00349G.

[31] W. Zimmermann et al., "Optical conductivity of BCS superconductors with arbitrary purity," *Physica C: Supercond.*, vol. 181, no. 1, pp. 99–104, Nov. 1991, doi: 10.1016/0921-4534(91)90771-P.

[32] Teracalc software, 2014. Accessed: Dec. 5, 2023. [Online]. Available: http://thzsoftware.com/teracalc/doku.php

[33] N. V. Kinev, A. M. Chekushkin, F. V. Khan, and K. I. Rudakov, "Study of superconducting transmission lines and tunnel junctions for signal detection at frequencies above 1 THz," *J. Commun. Technol. Electron.*, vol. 68, no. 9, pp. 946–951, Nov. 2023, doi: 10.1134/S1064226923090127.

[34] M. Born and E. Wolf, *Principles of Optics*. Cambridge, U.K.: Cambridge Univ. Press, 1999, pp. 64–71.

[35] M. Dressel and G. Gruner, *Electrodynamics of Solids*. Cambridge, U.K.: Cambridge Univ. Press, 2002.